Pressure-Induced 18 K Superconductivity and Two Superconducting Phases in $CuIr_2S_4$

Bijuan Chen[1*], Yuhao Gu[2], Dong Wang[1], Dexi Shao[2,9], Wen Deng[1], Xin Han[2], Meiling Jin[3], Jing Song[2], Yu Zeng[2], Hirofumi Ishii[4], Yen-Fa Liao[4], Dongzhou Zhang[5], Jianbo Zhang[1], Youwen Long[2,8], Jinlong Zhu[3], Liuxiang Yang[1], Hong Xiao[1], Jia-Cai Nie[6], Youguo Shi[2], Changqing Jin[2], Jiangping Hu[2*], Ho-kwang Mao[1,7], Yang Ding[1*]

[1] Center for High Pressure Science & Technology Advanced Research, Beijing, 100193, China
[2] Institute of Physics, Chinese Academy of Sciences, Beijing 100190, China
[3] Department of Physics and Shenzhen Engineering Research Center for Frontier Materials Synthesis at High Pressures, Southern University of Science and Technology (SUSTech), Shenzhen 518055, China
[4] National Synchrotron Radiation Research Center, Hsinchu 30076, Taiwan
[5] Hawaii Institute of Geophysics & Planetology, University of Hawaii Manoa, Honolulu, HI 96822, USA
[6] Department of Physics, Beijing Normal University, Beijing 100875, China
[7] Shanghai Advanced Research in Physical Sciences (SHARPS), Shanghai 201208, China
[8] Songshan Lake Materials Laboratory, Dongguan, Guangdong 523808, China
[9] School of Physics, Hangzhou Normal University, Hangzhou 311121, China

*To whom correspondence should be addressed; E-mail: bijuanchen.5459@gmail.com; jphu@iphy.ac.cn; yang.ding@hpstar.ac.cn

METHODS

Single crystal growth and characterization. The high-quality single crystals of $CuIr_2S_4$ used in our measurements were grown by a flux method and the structural parameters at ambient conditions were obtained by single-crystal X-ray diffraction. Single crystals of $CuIr_2S_4$ were grown from bismuth (Bi) solution and the details can be found elsewhere [1]. $CuIr_2S_4$ powders were first synthesized by a solid-state reaction method. To synthesize $CuIr_2S_4$ powders, high-purity powders of Cu (99.99%), Ir (99.99%) and S (99.999%) were sealed into an evacuated quartz tube and sintered at 850 °C for 3 d. Then, the prepared $CuIr_2S_4$ powders and high-purity Bi (99.99%) were mixed together in a $CuIr_2S_4$:Bi ratio of 1:100, and sealed into an evacuated quartz tube. The mixture was first heated to 1100 °C for 50 h and then slowly cooled down to 550 °C at a rate of 2 °C/h to grow the single crystals. Large crystals with sizes of several millimeters were obtained from the Bi flux by centrifuging at 550 °C. The samples were characterized by single-crystal XRD measurements using a Bruker D8 Quest diffractometer equipped with Mo Kα radiation. The data reduction, structure solution, and refinement were carried out with program APEX3[2, 3]. The refinement details can be found in the Supporting Information (Tables S I-v), in agreement with previous studies[1, 4].

High-pressure synchrotron PXRD measurements. The high-pressure synchrotron PXRD measurements up to 40.1 GPa (run 1) were performed at room temperature at beamline BL12B2 of SPring-8 with an 18 keV (λ = 0.68883 Å) beam to verify the phases and volume of $CuIr_2S_4$. A symmetric DAC was used to generate pressure with a pair of 400 µm culet-size anvils. A T301 stainless-steel gasket pre-pressed to 40 µm thickness with a 150 µm sample chamber was used. An appropriate amount of $CuIr_2S_4$ powder, ground from single crystals, was loaded into the pressure chamber with Ne gas as the pressure-transmitting medium. The pressure was determined via monitoring the fluorescence of ruby near the sample. The sample-to-detector distance and other detector parameters were calibrated using the CeO_2 standard. The diffraction images were integrated using the Dioptas program[5] and structure refinements were conducted by the Rietveld method in the General Structure Analysis System (GSAS)[6]. The ultra-high-pressure synchrotron PXRD experiments up to 219 GPa (run 2) were performed at beamline 13BM-C of GeoSoilEnviroCARS (GSECARS) at the Advanced Photon Source (APS), Argonne National Laboratory (ANL). The wavelength of the monochromatic X-ray beam was 0.434 Å. The diffraction patterns were collected by a MarCCD detector and integrated using Dioptas[5]. A symmetric DAC equipped with a pair of 100 µm culet-size anvils was used to generate pressure. A rhenium gasket, pre-indented to a thickness of 25 µm and featuring a 50 µm sample chamber, was employed. An appropriate amount of $CuIr_2S_4$ powder, ground from single crystals, was loaded into the pressure chamber.Neon gas was loaded into the pressure chamber as the pressure-transmitting medium to ensure quasi-hydrostatic conditions. Neon remains soft and provides a highly hydrostatic

environment up to 50–60 GPa, maintaining relatively low deviatoric stress even at higher pressures. The pressure was determined by monitoring the diffraction of a small piece of Au placed near the sample, using the known equation of state of Au. By analyzing the broadening of the Au Bragg reflections, we estimate the radial pressure gradient across the sample to be $\lesssim$ 2–3 GPa even in the 150–200 GPa range, supporting the conclusion that the observed phase-coexistence window (70 GPa) is unlikely to be an artifact of pressure inhomogeneity. The pressure was determined by monitoring the diffraction of a small piece of gold placed near the sample.

High-pressure X-ray single-crystal diffraction. The high-pressure X-ray single-crystal diffraction measurements were performed on $CuIr_2S_4$ single crystals up to 34.1 GPa at room temperature using a Bruker D8 Quest diffractometer equipped with Mo Kα radiation. Data were collected with a Sc-type DAC. Neon was used as the pressure-transmitting medium. The data reduction, structure solution, and refinement were carried out with program APEX3[2, 3].

Raman spectroscopy measurements. Raman spectra were collected in a backscattering geometry using a Renishaw Raman microscope. A laser excitation wavelength of 532 nm was used to obtain the sample's Raman spectra. The laser power was limited to less than 1.8 mW to avoid sample overheating. A single crystal of $CuIr_2S_4$ was chosen for measurement, and all Raman measurements were performed on the same surface. Neon was used as the pressure-transmitting medium and ruby fluorescence was used to calibrate the pressure.

High-pressure transport measurements. Symmetric anvil cells composed of BeCu with various culet sizes from 100 µm to 300 µm were used for high-pressure transport measurements. The Re gasket was pre-indented to 20 µm and then drilled with a hole of 290 µm diameter at the center of the imprint. Fine insulating cubic boron nitride (cBN) powders mixed with epoxy were filled into the hole and further pressed to form a solid layer of $\sim$ 15 µm thickness. A hole of 60 µm diameter was drilled at the center of the cBN layer to serve as the sample chamber. NaCl was chosen as the pressure-transmitting medium due to its stable insulating behavior under compression and its demonstrated suitability for resistivity measurements [7]. Although NaCl undergoes a phase transition at 26.8 GPa [8], this does not affect the resistivity of the sample, as NaCl remains non-metallic up to pressures exceeding 350 GPa [9].The four-probe method was applied for all measurements. Pt foils of 3 µm thickness were deposited on the culet surface as inner electrodes. Copper wires were attached to the Pt foils as outer electrodes. For each measurement cycle, the pressure was calibrated by ruby fluorescence shift and diamond Raman at room temperature. We acknowledge that non-hydrostatic stresses and pressure gradients, inevitable at these extreme pressures, may broaden the observed transitions. However, the coexistence range (70 GPa) is much larger than typical pressure gradients in such cells, which are generally of order a few to at most several gigapascals at 100–200 GPa. Furthermore, the simultaneous evolution of the structural Phase VI–VII transition and the SC-I to SC-II electronic crossover suggests that the coexistence is intrinsic to the material's phase-boundary dynamics, likely enhanced but not caused by pressure inhomogeneity. Transport measurements were performed on a Quantum Design PPMS with a magnetic field up to 9 T and temperature from 2 to 300 K. Higher magnetic field measurements (9–14 T) were carried out in a homemade multifunctional measurement system (1.5–300 K, PHYSIKE Inc.; 0–14 T, Cryomagnetics Inc.). Temperature-dependent electrical resistance measurements $R(T)$ at ambient pressure confirm a metal-insulator transition (MIT) upon cooling, as shown in Fig. S1a, aligning with previous findings[10, 11].

First-principles calculations. Density functional theory (DFT) calculations were performed using the Vienna *ab initio* simulation package (VASP)[12] with the projector augmented-wave (PAW) method[13]. The Perdew–Burke–Ernzerhof (PBE) exchange-correlation functional[14] was used. This approach tends to underestimate the absolute value of the band-gap energy but gives a good description of its pressure dependence[15]. The kinetic energy cutoff was set to 600 eV for the plane-wave basis and the energy convergence criterion was 10^{-6} eV. Monkhorst–Pack k-meshes of $8\times8\times8$, $6\times8\times6$, $8\times8\times8$, and $8\times8\times8$ were used for $CuIr_2S_4$ under 0, 5.4, 14.1, and 21.4 GPa, respectively. All crystal structures were fully relaxed until forces were less than 0.005 eV/Å.

ANISOTROPY TRANSPORT

It is notable that we observe the emergence of in-plane (111) resistance anisotropy in the SC-I phase, as evidenced by van der Pauw measurements (inset Fig.S6a). A small single crystal was selected with its [111] axis aligned parallel to the diamond culet, enabling direct probing of in-plane electronic responses under pressure. At 49.5 GPa, the resistance exhibits insulating behavior above $T_c^{\text{SC-I}}$ when current is applied between electrodes 3 and 4 (denoted R_{12}), while it shows less insulating behavior when current is applied between 2 and 3 (marked R_{14}). Below $T_c^{\text{SC-I}}$, R_{14} abruptly increases by ∼130 %, whereas R_{12} decreases by ∼86 %. Although the van der Pauw geometry may amplify anisotropy, the observed trends are robust and reproducible. Interestingly, when we randomly polished the sample surface such that multiple crystal orientations were exposed on the top surface facing the diamond culet where electrodes were placed, a metallic behavior was observed in R_{12} above $T_c^{\text{SC-I}}$ at pressures above 18 GPa (Fig. S1c). Such pronounced resistance anisotropy signals the onset of a macroscopic phase that breaks in-plane rotational symmetry[16, 17].

$CuIr_2S_4$ therefore undergoes a rare, direct transition from a transport-anisotropic state to superconductivity, bypassing the conventional intermediate metallic phase. This contrasts sharply with most known spinel-derived superconductors, such as lacunar spinels GaM_4X_8 (M = Nb, Ta; X = S, Se), which typically follow an insulator–metal–superconductor sequence. Interestingly, when we randomly polished the sample surface such that multiple crystal orientations were exposed on the top surface facing the diamond culet where electrodes were placed, a metallic behavior was observed in R_{12} above $T_c^{\text{SC-I}}$ under pressures above 18GPa. This metallic behavior is progressively suppressed with increasing pressure, reverting to insulating behavior above 27GPa.

To further explore this anisotropy, we applied magnetic fields perpendicular to the sample-111 plane and measured R_{14} and R_{12} (Figs. S6b and S6c). Below $T_c^{\text{SC-I}}$, R_{14} decreases (negative MR) while R_{12} increases (positive MR) (see Fig. S1d). Above $T_c^{\text{SC-I}}$, both resistances converge to the normal state (white background), and MR anisotropy vanishes, reminiscent of a stripe-like phase suppressed by field[17, 18]. This in-plane anisotropy remains in SC-I until SC-II onset, where both R_{14} and R_{12} drop to zero at $T_c^{\text{SC-II}}$ (pink background, Figs. S6d–S6i). The SC-I anisotropy weakens above 133.3 GPa, disappears beyond 199 GPa (Fig. S6h), and intriguingly reemerges at pressures above 224 GPa (Figs. S6i and S7).

The in-plane anisotropy and its suppression under magnetic field resemble electronic stripe-like or nematic behavior, as seen in 2D granular superconductors and high-T_c cuprates such as $Bi_2Sr_2CaCu_2O_{8+\delta}$ [19]. These findings point to a possible competing or coexisting order parameter in the SC-I phase, potentially related to spin-density wave formation, charge ordering, or orbital polarization. The interplay between superconductivity and broken symmetry in $CuIr_2S_4$ underscores its potential as a model platform for studying unconventional pairing in frustrated lattice systems.

[1] N. Matsumoto and S. Nagata, J. Cryst. Growth **210**, 772 (2000).
[2] Bruker, Bruker AXS Inc. (2009).
[3] G. M. Sheldrick, Acta Crystallogr. A **71**, 3 (2015).
[4] T. Furubayashi, T. Matsumoto, T. Hagino, and S. Nagata, J. Phys. Soc. Jpn. **63**, 3333 (1994).
[5] C. Prescher and V. B. Prakapenka, High Press. Res. **35**, 223 (2015).
[6] B. H. Toby and R. B. Von Dreele, J. Appl. Crystallogr. **46**, 544 (2013).
[7] D. Errandonea, D. Martínez-García, A. Segura, A. Chevy, G. Tobias, E. Canadell, and P. Ordejon, Phys. Rev. B **73**, 235202 (2006).
[8] X. Li and R. Jeanloz, Phys. Rev. B **36**, 474 (1987).
[9] X. Chen and Y. Ma, Europhys. Lett. **100**, 26005 (2012).
[10] A. B. Garg, V. Vijayakumar, B. K. Godwal, A. Choudhury, and H. D. Hochheimer, Solid state communications **142**, 369 (2007).
[11] S. Nagata, T. Hagino, Y. Seki, and T. Bitoh, Physica B **194**, 1077 (1994).
[12] G. Kresse and J. Furthmüller, Comput. Mater. Sci. **6**, 15 (1996).
[13] G. Kresse and D. Joubert, Phys. Rev. B **59**, 1758 (1999).
[14] J. P. Perdew, K. Burke, and M. Ernzerhof, Phys. Rev. Lett. **77**, 3865 (1996).
[15] T. Ouahrani, R. M. Boufatah, M. Benaissa, Á. Morales-García, M. Badawi, and D. Errandonea, Phys. Rev. Mater. **7**, 025403 (2023).
[16] V. Barzykin and L. P. Gor'kov, Phys. Rev. Lett. **89**, 227002 (2002).

[17] C. Liu, X. Yan, D. Jin, Y. Ma, H. W. Hsiao, Y. Lin, T. M. Bretz-Sullivan, X. Zhou, J. Pearson, B. Fisher, and J. S. Jiang, Science **371**, 716 (2021).
[18] M. Jin, P. Yu, C. Fan, Q. Li, P. Kong, Z. Shen, X. Qin, Z. Chi, C. Jin, G. Liu, G. Zhong, G. Xu, Z. Liu, and J. Zhu, Adv. Sci. **8**, e2103250 (2021).
[19] J. Guo, Y. Zhou, C. Huang, S. Cai, Y. Sheng, G. Gu, C. Yang, G. Lin, K. Yang, A. Li, Q. Wu, T. Xiang, and L. Sun, Nat. Phys. **16**, 295 (2019).
[20] J. Zwinscher and H. Lutz, J. Alloys Compd. **219**, 103 (1995).
[21] B. Ammundsen, G. R. Burns, M. S. Islam, H. Kanoh, and J. Rozière, J. Phys. Chem. B **103**, 5175 (1999).
[22] L. Zhang, L. S. Ling, Z. Qu, W. Tong, S. Tan, and Y. H. Zhang, Eur. Phys. J. B **77**, 83 (2010).
[23] M. Naseska, P. Sutar, D. Vengust, S. Tsuchiya, M. Čeh, D. Mihailovic, and T. Mertelj, Phys. Rev. B **101**, 165134 (2020).

ACCESSION CODES

CCDC 2347018, 2347000, 2347001 contain the supplementary crystallographic data for this paper. These data can be obtained free of charge via `www.ccdc.cam.ac.uk/data_request/cif`, or by emailing data_request@ccdc.cam.ac.uk, or by contacting The Cambridge Crystallographic Data Centre, 12 Union Road, Cambridge CB21EZ, UK; fax: +44 1223336033.

Table S I: The experimental single crystal X-ray diffraction and structure determination details of $CuIr_2S_4$ under different pressures.

Pressure	1 atm	14.13 GPa	21.41 GPa
CCDC No.	2347018	2347000	2347001
X-ray wavelength (Å)	0.71073	0.71073	0.71073
Pressure medium	—	Ne	Ne
Fw (g/mol)	576.18	576.18	2304.72
Crystal system	Cubic	Triclinic	Orthorhombic
Space group	$Fd\bar{3}m$	$P\bar{1}$	$Imma$
a (Å)	9.8677 (15)	6.611 (3)	6.744 (3)
b (Å)	9.8677 (15)	6.638 (3)	6.953 (10)
c (Å)	9.8677 (15)	6.831 (9)	9.474 (6)
α (deg.)	90	61.14 (7)	90
β (deg.)	90	61.56 (7)	90
γ (deg.)	90	61.89 (2)	90
V (Å^3)	960.8 (4)	219.2 (4)	444.3 (7)
Z	8	8	1
ρ_c (g/cm^3)	7.966	8.730	8.614
μ (mm^{-1})	61.20	67.07	66.18
Measured reflections	541	406	559
Observed $[I > 2\sigma(I)]$	45	145	123
Independent reflections	45	104	74
Refined parameters	7	25	12
$R_{\rm int}$	0.047	0.060	0.088
$R_1[I > 2\sigma(I)]$	0.025	0.121	0.186
wR_2 (all data)	0.034	0.347	0.495
S	1.54	1.50	1.98
$\theta_{\rm max}, \theta_{\rm min}$ (deg)	22.8°, 3.6°	26.4°, 3.7°	27.7°, 3.6°
$\Delta\rho_{\rm max}, \Delta\rho_{\rm min}$ (e Å^{-3})	1.47, -1.56	2.96, -2.48	5.16, -7.76

Table S II: Fractional atomic coordinates and isotropic or equivalent isotropic displacement parameters (Å^2) of $CuIr_2S_4$ at 1 atm.

Atom	x	y	z	U_{iso}*/U_{eq}
Ir	1/2	1/2	1/2	0.0065 (5)
Cu	7/8	3/8	3/8	0.0107 (8)
S	0.7397 (2)	0.5103 (2)	0.5103 (2)	0.0076 (13)

Table S III: The experimental powder crystal X-ray diffraction and structure determination details of $CuIr_2S_4$ at 5.4 GPa. The structure was determined from powder-crystal (grind from single crystal sample) data in the $P\bar{1}$ space group (No. 2, Setting 1). The wavelength of the monochromatic X-ray beam is 0.688 83 Å. Lattice parameters are: $a = 11.810\,98$ Å, $b = 6.905\,83$ Å, $c = 11.811\,13$ Å, $\alpha = 91.1258°$, $\beta = 108.4129°$, $\gamma = 91.0649°$, $V = 913.562\,393$ Å^3. All atoms were refined with full occupancy as listed.

Atom	x	y	z	Atom	x	y	z
Cu1	0.95549	0.26152	0.04096	Ir8	0.74549	0.24521	0.49001
Cu2	0.06597	0.28435	0.46564	S1	0.24744	0.43116	0.92453
Cu3	0.53708	0.24666	0.90843	S2	0.25733	-0.02536	0.89421
Cu4	0.43700	0.25460	0.56430	S3	0.16184	0.97675	0.39780
Ir1	0.24984	-0.00695	0.74942	S4	0.07190	0.53917	0.36039
Ir2	0.24340	1.02529	0.23323	S5	0.60810	0.99130	0.86160
Ir3	0.27595	0.24642	1.01972	S6	0.65595	0.50997	0.85171
Ir4	-0.01562	0.21288	0.74955	S7	0.63180	0.47140	0.37190
Ir5	0.23353	0.48918	0.74296	S8	0.63870	0.00800	0.37260
Ir6	0.25911	0.52304	0.28232	S9	0.87163	0.22791	1.37727
Ir7	0.51945	0.24577	0.27018	S10	0.65558	0.23999	0.16482
S11	0.10246	0.26132	0.09820	S12	0.34510	0.25721	0.33575
S13	0.61145	0.23500	0.60933	S14	0.86325	0.23586	0.86045
S15	0.30701	0.24680	0.82276	S16	0.15047	0.24285	0.65533

Table S IV: Fractional atomic coordinates and isotropic or equivalent isotropic displacement parameters (Å^2) of $CuIr_2S_4$ at 14.13 GPa.

Atom	x	y	z	U_{iso}*/U_{eq}
Ir1	3/2	1/2	0	0.056 (4)*
Ir2	3/2	0	0	0.032 (3)*
Ir3	1/2	1/2	1/2	0.029 (3)*
Ir4	1	1/2	0	0.032 (3)*
Cu	0.130 (4)	0.129 (4)	0.600 (13)	0.035 (5)*
S1	0.717 (11)	0.272 (9)	0.30 (3)	0.039 (11)*
S2	1.263 (10)	0.249 (9)	0.23 (3)	0.024 (10)*
S3	0.261 (13)	0.731 (11)	0.28 (3)	0.050 (13)*
S4	0.745 (8)	0.760 (7)	0.21 (2)	0.014 (8)*

Table S V: Fractional atomic coordinates and isotropic or equivalent isotropic displacement parameters (Å^2) of $CuIr_2S_4$ at 21.41 GPa.

Atom	x	y	z	U_{iso}*/U_{eq}
Ir1	1/2	1/2	1	0.062 (5)*
Ir2	1/4	3/4	1/4	0.055 (6)*
Cu	1/2	3/4	0.624 (4)	0.077 (11)*
S1	1/2	0.459 (17)	0.769 (8)	0.10 (2)*
S2	0.196 (10)	3/4	0.485 (9)	0.11 (2)*

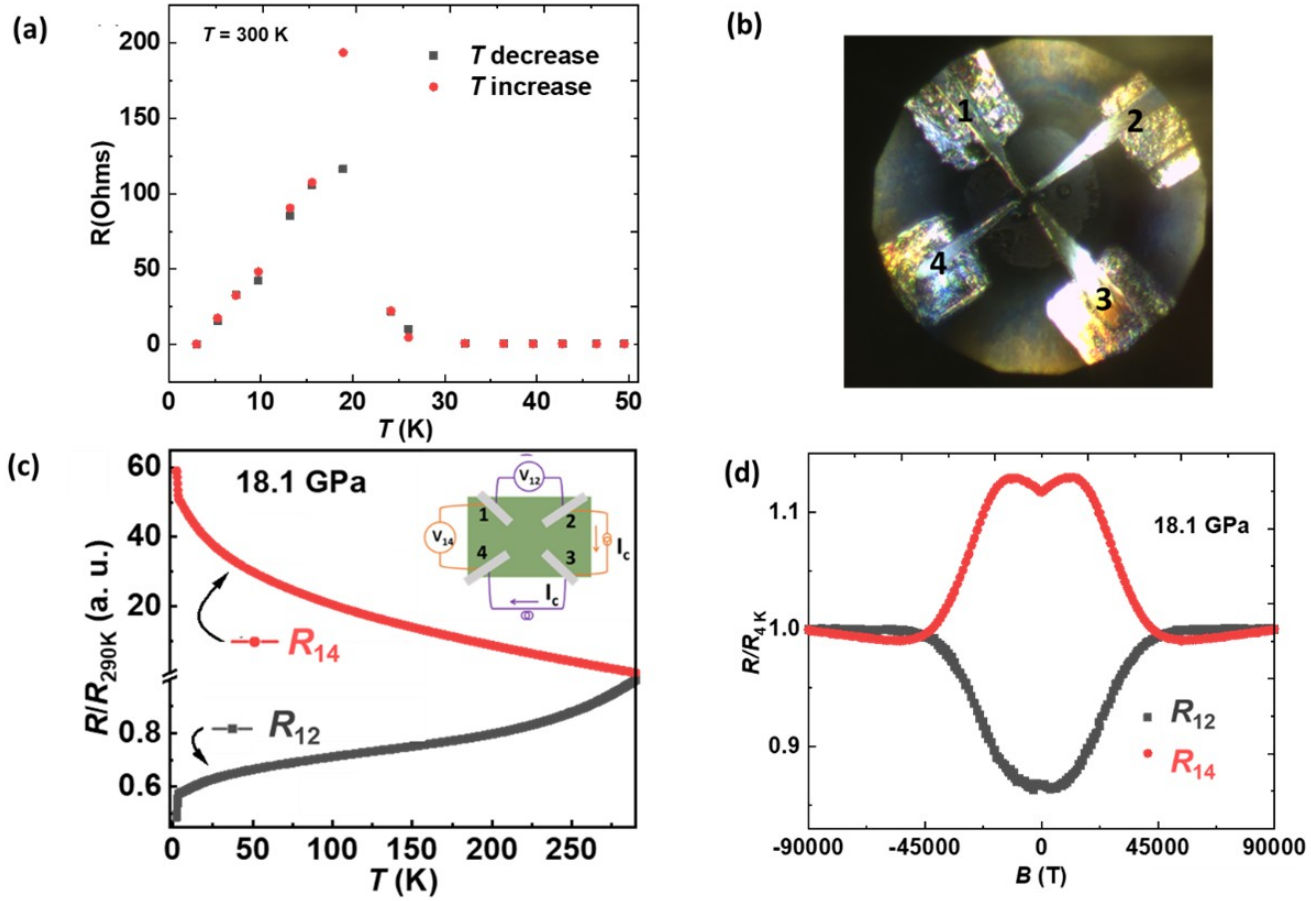

Fig.S 1: (a) Electrical resistance of $CuIr_2S_4$ as a function of pressure at room temperature, showing consistency with previous reports [10] up to 49.5 GPa. (b) Optical image of single crystal sample S2 under a microscope at 18.1 GPa. The $CuIr_2S_4$ crystal (center) is embedded in NaCl pressure medium and enclosed by a cubic BN gasket. Four electrodes are placed on a polished surface with multiple crystallographic orientations. (c) Temperature dependence of resistance (R_{12} and R_{14}) at 18.1 GPa from sample S2. Inset illustrates the electrode configuration used for simultaneous measurement of R_{12} and R_{14}. (d) Magnetic field dependence of normalized resistance ($R/R_{4\,\mathrm{K}}$) for R_{12} and R_{14} measured at $T = 4$ K and $P = 18.1$ GPa, indicating anisotropic magnetoresistance behavior.

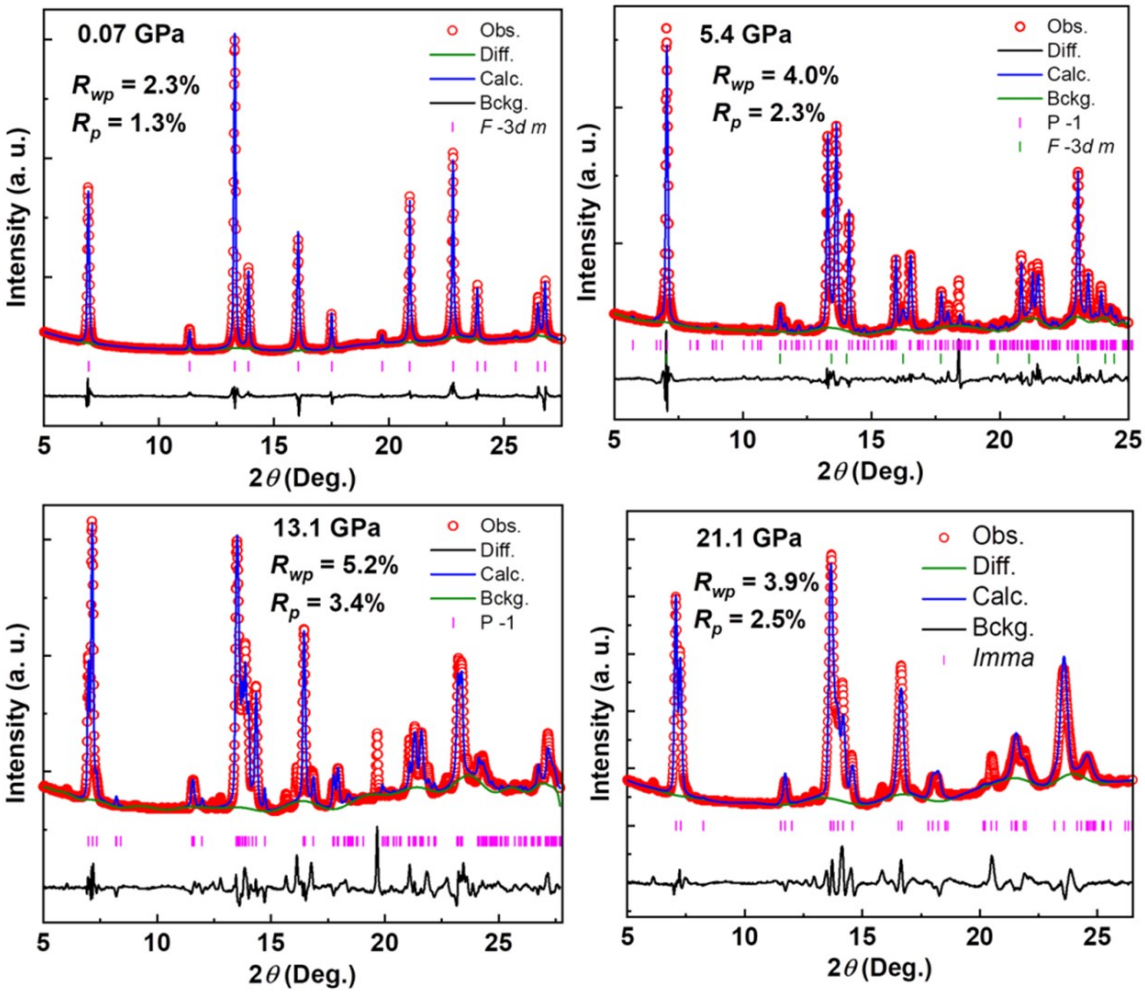

Fig.S 2: Example of Rietveld refinement of the XRD patterns of $CuIr_2S_4$ collected at 0.07, 5.4, 13.1 and 21.1 GPa for the $Fd\bar{3}m$, $P\bar{1}$ (phase II), $P\bar{1}$ (phase III) and $Imma$ space groups, respectively.

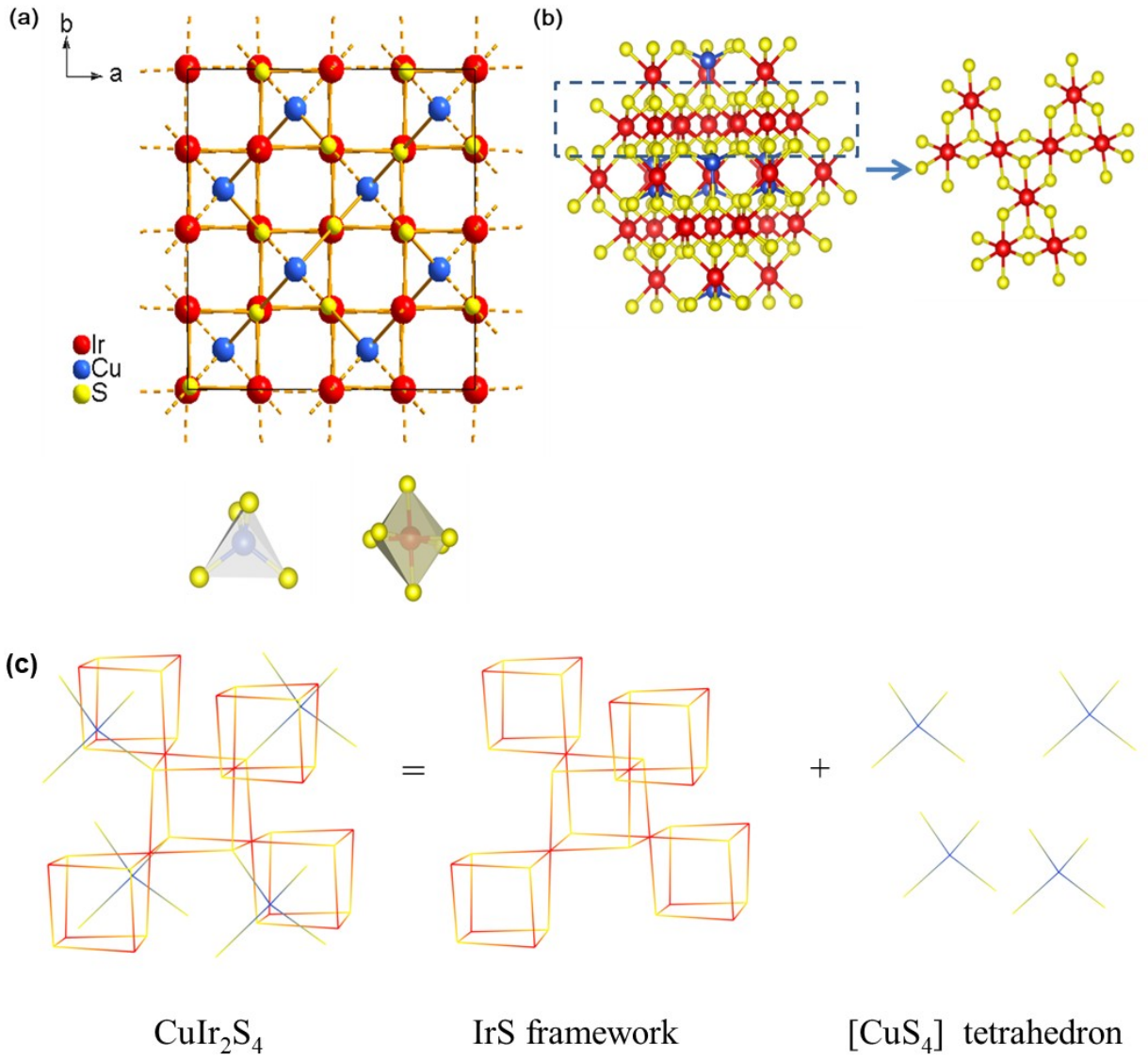

Fig.S 3: Crystal structure of $CuIr_2S_4$ (a) viewed along the c axis, (b) enlarged view of Ir-S layer in compound $CuIr_2S_4$ at ambient pressure, respectively. (c) Spinel structural units are differentiated with $[IrS_6]$ framework and $[CuS_4]$ tetrahedron.

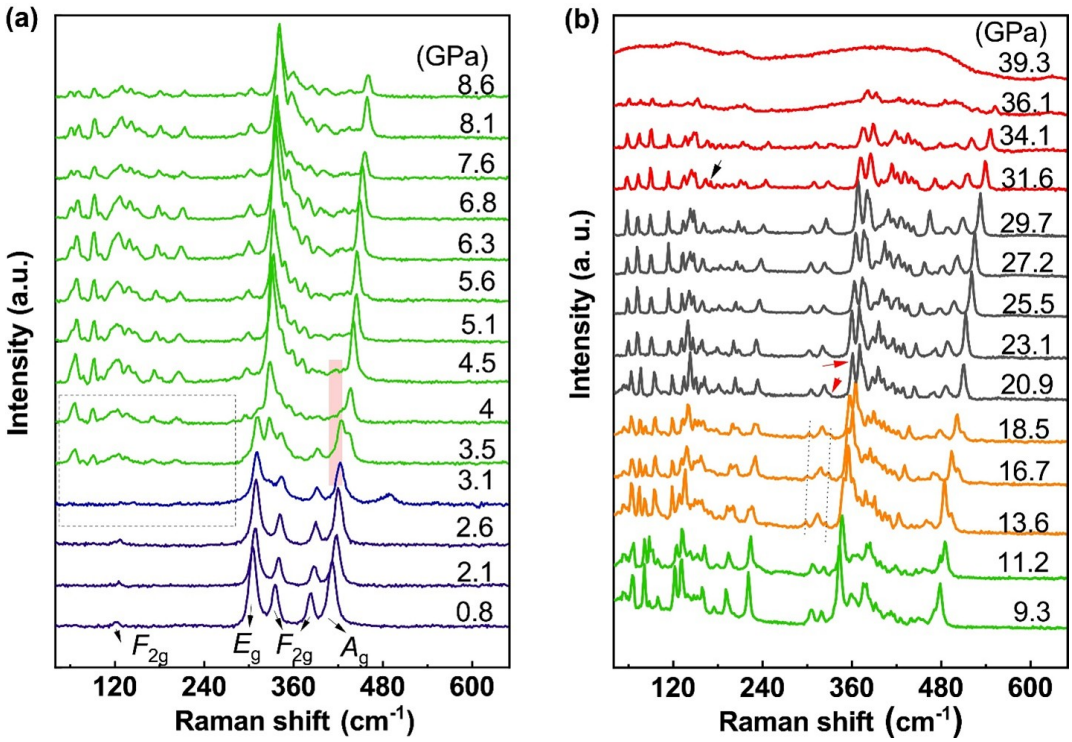

Fig.S 4: Selected room-temperature pressure-dependent Raman spectra from cleaved single crystal surface of $CuIr_2S_4$ taken in the backscattering geometry using a 532 nm wavelength. The measuring time of 60 s and 20 accumulations were kept constant for all spectra. Initially, the $CuIr_2S_4$ crystal exhibits a cubic normal spinel-type structure with space group $Fd\bar{3}m$ (No. 227) form, producing five Raman active modes [20, 21]: $1A_{1g} + 1E_g + 3F_{2g}$. Though typically unobservable, the $3F_{2g}(3)$ mode is seen on cleaved surfaces, leading to a detection of five vibration modes, aligning with prior findings [22, 23]. Below 3.1 GPa, the Raman spectra show minor changes, except for a blue shift symbolizing increased vibrational strength under pressure. At 4 GPa, new Raman peaks emerge, and F_{2g} modes fade, indicating a transition towards the insulator state and chemical dimerization of Ir-Ir bonds. Around 13.6 GPa, a distinct Raman peak at 300 cm^{-1} coincides with the transition from phase II to III. Further pressure changes affect other Raman modes, with peak strengthening observed at 20.9 GPa. Collectively, these Raman data corroborate PXRD and electrical transport results, validating four phase transitions below 40 GPa. By 39.3 GPa, Raman modes almost disappear, marking an approach to a new metallic state. It should be noted that these observed changes are reversible when the sample is released to the ambient pressure.

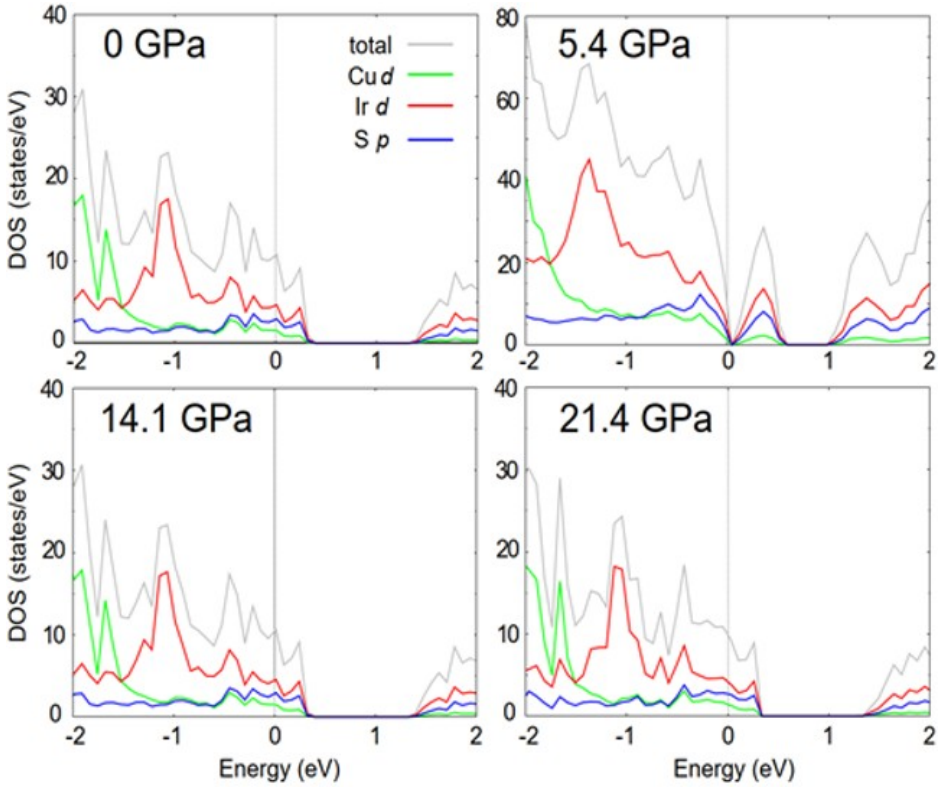

Fig.S 5: Total (gray) and momentum-projected DOS on Ir-d (red), Cu-d (green), and S-p (blue) spherical harmonics at different pressures.

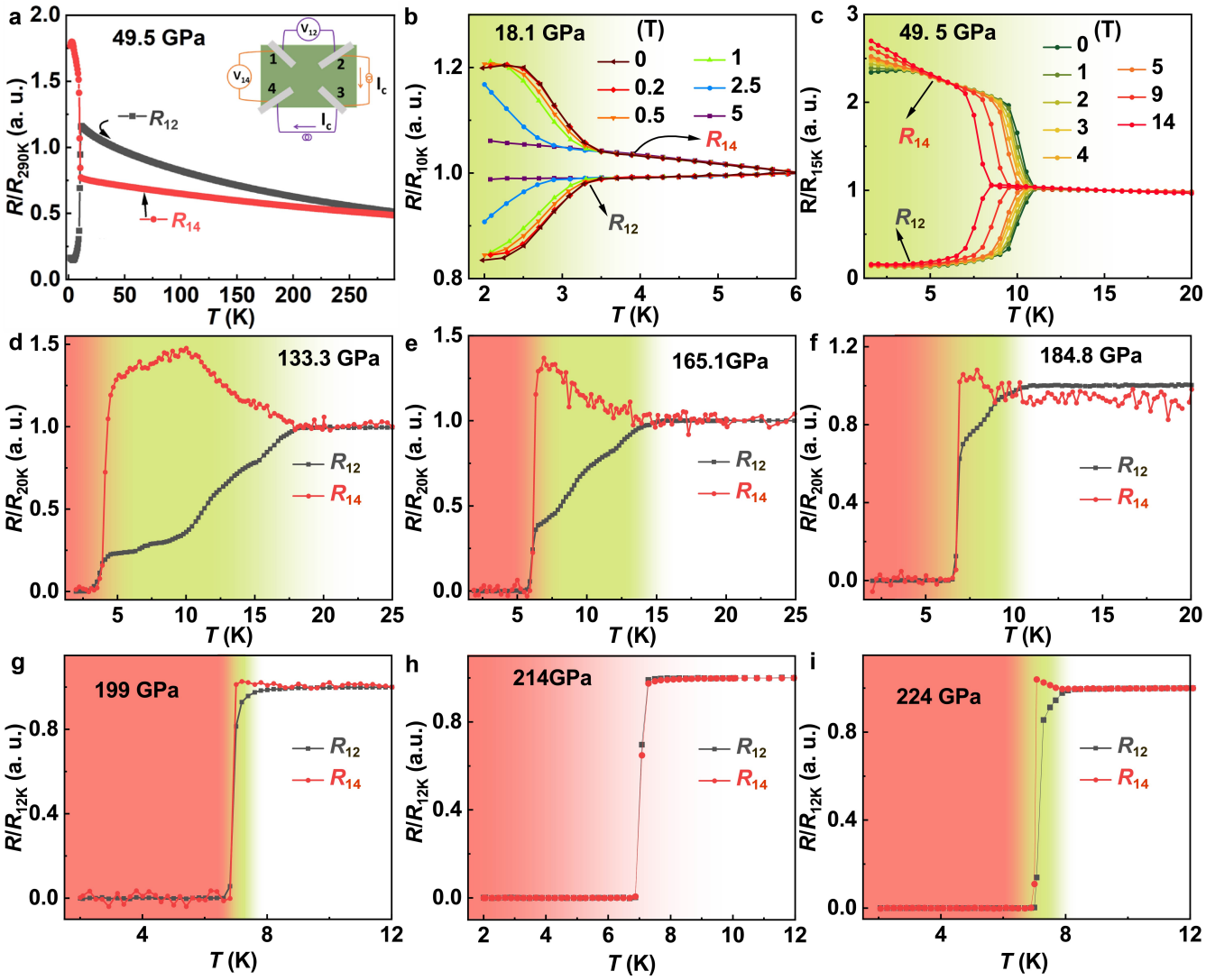

Fig.S 6: R_{12} and R_{14} as a function of temperature in $CuIr_2S_4$ under varying pressures. (**a**) $R_{12}(T)$ and $R_{14}(T)$ measured at 49.5 GPa. Inset of (**a**) shows the integration of electrodes for concurrent measurements of $R_{12}(T)$ and $R_{14}(T)$. (**b**, **c**) Magnetic field dependence of superconducting transition temperatures measured along both current directions at 18.1 GPa and 49.5 GPa, respectively. (**d**–**i**) $R_{12}(T)$ and $R_{14}(T)$ measured at pressures of 133.3 GPa (**d**), 165.1 GPa (**e**), 184.8 GPa (**f**), 199 GPa (**g**), 214 GPa (**h**) and 224 GPa (**i**). Pink zones indicate the zero-resistance superconducting state, and green zones represent the "stripe-like" phase.

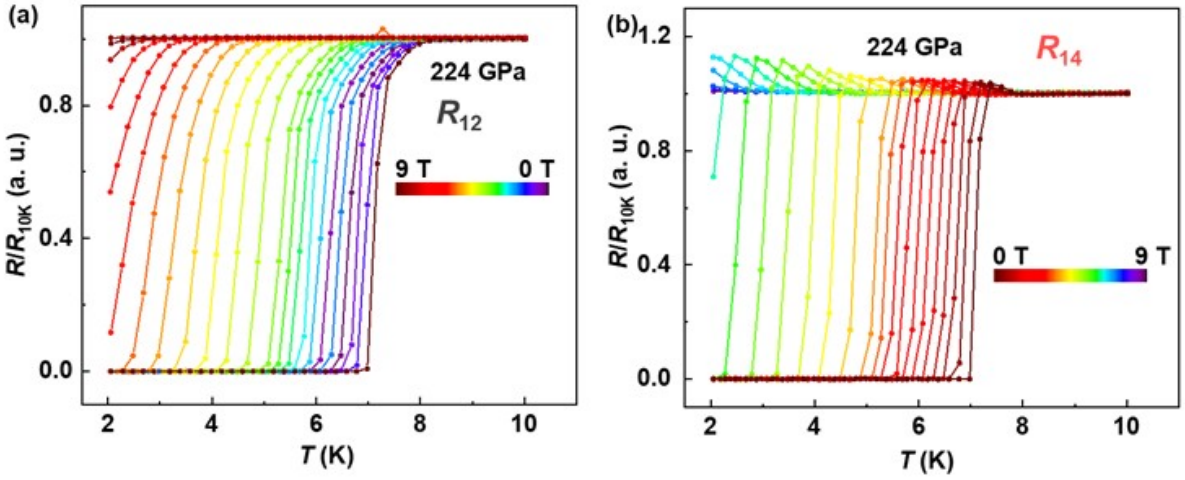

Fig.S 7: R_{12} and R_{14} measured at pressure of 224 GPa.

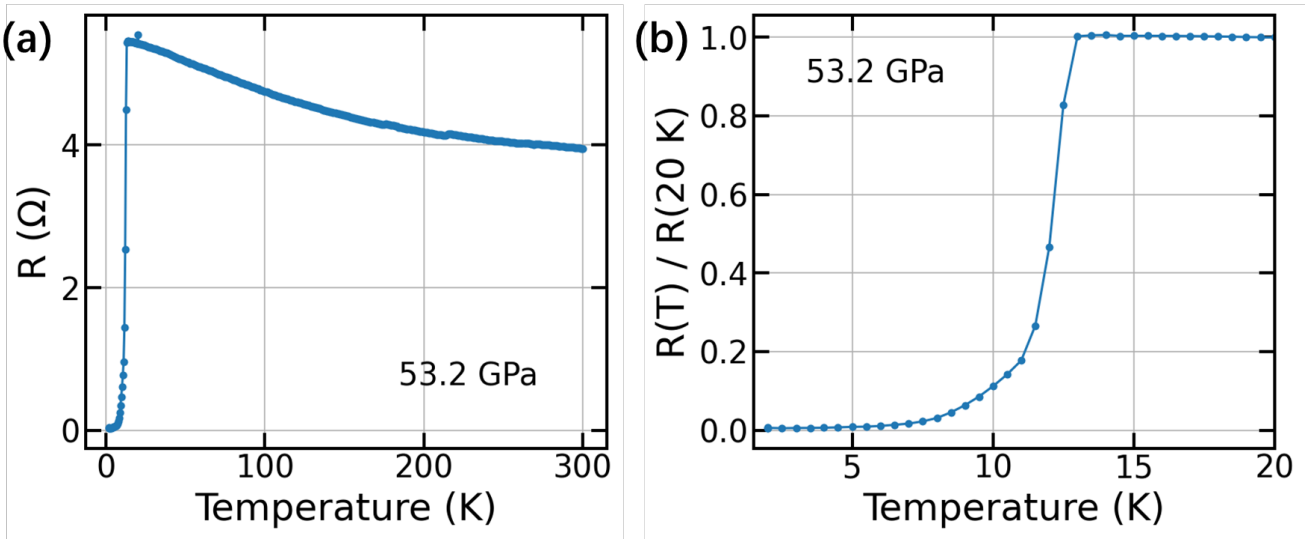

Fig.S 8: Temperature dependence of resistance of $CuIr_2S_4$ at 53.2 GPa. At 53.2 GPa, the resistance drops by nearly $98\% R/R_{20K}$ from 1 to 0.02, making a simple magnetic-ordering transition unlikely, as such transitions typically manifest only as minor kinks or slope changes.